AIP | The Journal of Chemical Physics

Diffusion, sedimentation, and rheology of concentrated suspensions of core-shell particles

Gustavo C. Abade, Bogdan Cichocki, Maria L. Ekiel-Jeżewska, Gerhard Nägele, and Eligiusz Wajnryb

Citation: J. Chem. Phys. **136**, 104902 (2012); doi: 10.1063/1.3689322
View online: http://dx.doi.org/10.1063/1.3689322
View Table of Contents: http://jcp.aip.org/resource/1/JCPSA6/v136/i10
Published by the American Institute of Physics.

Diffusion, sedimentation, and rheology of concentrated suspensions of core-shell particles

Gustavo C. Abade,[1] Bogdan Cichocki,[2] Maria L. Ekiel-Jeżewska,[3,a)] Gerhard Nägele,[4] and Eligiusz Wajnryb[3]
[1]*Departamento de Engenharia Mecânica, Faculdade de Tecnologia, Universidade de Brasília, Campus Universitário Darcy Ribeiro, 70910-900 Brasília-DF, Brazil*
[2]*Institute of Theoretical Physics, Faculty of Physics, University of Warsaw, Hoża 69, 00-681 Warsaw, Poland*
[3]*Institute of Fundamental Technological Research, Polish Academy of Sciences, Pawińskiego 5B, 02-106 Warsaw, Poland*
[4]*Institute of Complex Systems (ICS-3), Research Centre Jülich, D-52425 Jülich, Germany*

(Received 27 December 2011; accepted 7 February 2012; published online 9 March 2012)

Short-time dynamic properties of concentrated suspensions of colloidal core-shell particles are studied using a precise force multipole method which accounts for many-particle hydrodynamic interactions. A core-shell particle is composed of a rigid, spherical dry core of radius a surrounded by a uniformly permeable shell of outer radius b and hydrodynamic penetration depth κ^{-1}. The solvent flow inside the permeable shell is described by the Brinkman-Debye-Bueche equation, and outside the particles by the Stokes equation. The particles are assumed to interact non-hydrodynamically by a hard-sphere no-overlap potential of radius b. Numerical results are presented for the high-frequency shear viscosity, η_∞, sedimentation coefficient, K, and the short-time translational and rotational self-diffusion coefficients, D_t and D_r. The simulation results cover the full three-parametric fluid-phase space of the composite particle model, with the volume fraction extending up to 0.45, and the whole range of values for κb, and a/b. Many-particle hydrodynamic interaction effects on the transport properties are explored, and the hydrodynamic influence of the core in concentrated systems is discussed. Our simulation results show that for thin or hardly permeable shells, the core-shell systems can be approximated neither by no-shell nor by no-core models. However, one of our findings is that for $\kappa(b-a) \gtrsim 5$, the core is practically not sensed any more by the weakly penetrating fluid. This result is explained using an asymptotic analysis of the scattering coefficients entering into the multipole method of solving the Stokes equations. We show that in most cases, the influence of the core grows only weakly with increasing concentration. © *2012 American Institute of Physics*. [http://dx.doi.org/10.1063/1.3689322]

I. INTRODUCTION

Suspensions of composite colloidal particles are of relevance in many biomedical and technological applications. An important subset of composite systems is formed by globular core-shell particles composed of a solid, dry core, and a solvent-permeable spherical shell. The shell consists typically of some soft material such as grafted polymers whose internal structure may change with concentration. There exists a large variety of core-shell particle systems.[1–10] An example of practical relevance is that of polymer-grafted nanoparticles which play a role in the development of photonic and nanocomposite materials. The polymer coating stabilizes the suspension against flocculation, which otherwise may be induced by the van der Waals attraction in the absence of additional stabilizing mechanisms. Another system of practical relevance is formed by core-shell particles with a magnetically polarizable core which are used in magnetorheological applications and for drug targeting.[11]

Core-shell particles can be considered as intermediates between hard, non-permeable particulate systems such as polymethylmetacrylate (i.e., plexiglass) particles,[12] and soft systems such as star polymers.[13] To understand the rheology and diffusion in non-dilute core-shell systems, the consideration of solvent-mediated hydrodynamic interactions (HIs) between the particles is of central importance. The theoretical treatment of the HIs is complicated by the fact that the solvent can penetrate the permeable shell. Two important consequences of the shell permeability are the enhanced coagulation kinetics of attractive particles, and the suppression of shear-thickening in concentrated suspensions subject to strong shear flow.[14]

Since the treatment of HIs in core-shell particle suspensions is difficult, the theoretical work performed so far centers around single-particle hydrodynamics, and the HIs between isolated pairs of particles. In contrast to this, little is known about diffusion and rheological transport properties in concentrated suspensions, where many-particle HIs are strong. In most of the theoretical work on the dynamics of core-shell particles, the flow inside a permeable shell is described using the Brinkman-Debye-Bueche (BDB) equation[15,16] for a constant permeability coefficient. More structure can be introduced, for example by allowing

a)Electronic mail: mekiel@ippt.gov.pl.

for a radially symmetric permeability profile,[17,18] which in principle can be related to the radial polymer density profile in the shell.[19,20]

Masliyah *et al.*[1] have derived an analytic expression for the translational friction coefficient of an isolated sphere of arbitrary shell width but constant permeability. A detailed analytical analysis of the intrinsic viscosity was given by Zackrisson and Bergenholtz.[21] Numerical results for the single-particle rotational diffusion coefficient of a core-shell particle were derived by Chen and Ye.[22] They also discuss Faxén theorems for the translational force and the symmetric force dipole exerted on the particle exposed to an arbitrary incident flow. Concise analytic expressions for all the scattering coefficients, including the translational and rotational friction coefficients and intrinsic viscosity of a core-shell sphere, and the related Faxén theorems, have been provided by Cichocki and Felderhof.[23]

A major conclusion drawn from the analysis of the single-particle properties is that a core-shell particle behaves like a uniformly porous sphere of equal permeability and equal outer radius when, at sufficiently low permeability, the fluid cannot penetrate deeply enough into the shell to sense the core surface.

The analysis of a single core-shell particle with constant shell permeability has been extended to fractal aggregates with radially symmetric permeability profiles.[24,25] The low-order friction coefficients of a spherical particle with an arbitrary radially symmetric permeability profile related to translation, rotation and intrinsic viscosity were calculated by Felderhof *et al.*[26,27] Friction coefficients for arbitrary angular dependence of the flow were derived by Jones and Schmitz.[28] Faxén theorems for the hydrodynamic force, torque, and symmetric force dipole of a sphere with radially symmetric permeability profile have been obtained by Felderhof and Jones.[17]

For particles with a very thin permeable shell, the determination of single-particle properties becomes more simple. Anderson and co-workers[29–31] used a matched asymptotic expansion to analyze the flow in a thin shell. They showed that a flow-type dependent influence on the single-particle transport coefficients appears only at quadratic order in the shell width to core size ratio $\epsilon = (b - a)/a$. To linear order in ϵ, the only effect of a uniform thin shell is to slightly expand the no-slip boundary at the core radius by the factor of $(1 + A\epsilon)$, where the so-called hydrodynamic layer width, $A\epsilon$, is independent of the nature of the flow.[30]

In addition to single-particle properties, the HIs between two core-shell particles were studied in greater detail. The method of reflections[30] and the boundary collocation method[32] have been used to investigate the translational hydrodynamic mobilities for composite spheres with a thin porous shell. Chen[33] calculated the drag force on up to four particles of arbitrary shell width in axisymmetric motion. He also performed a lubrication analysis showing that, in contrast to hard spheres with stick boundary conditions, the drag force remains finite when two approaching core-shell particles come into contact. We note here that a numerically efficient scheme has been derived in Refs. 28 and 34, which allows for the evaluation of translational, rotational, and force dipole related mobilities as a series expansion in the inverse two-particle center-to-center distance to be made. The scheme involves the single-particle friction coefficients as input, so that it is applicable to particles of general hydrodynamic structure such as core-shell spheres and droplets.

Calculations of transport properties of interacting core-shell particles, which require a statistical average over the particle distribution, are scarce. The high-frequency viscosity in the limit of low shear rate, and the large-shear-rate viscosity have been calculated by Russel *et al.*[19,20] and Nommensen *et al.*[35] In these calculations, a non-constant density profile of surface-grafted polymers was accounted for, but the HIs were treated in a simplifying lubrication approximation applicable at very high concentrations only.

In earlier work on concentrated suspensions of uniformly permeable particles, we have calculated a broad spectrum of short-time dynamic properties, amended by the derivation of analytic approximations of good accuracy.[40–44] The present work constitutes an important extension of this earlier work to composite particle systems.

The present paper reports the first comprehensive simulation study of short-time diffusion and rheological properties of concentrated suspensions of core-shell particles. An individual particle is composed of a rigid spherical core of radius a, surrounded by a uniformly permeable, incompressible shell of outer radius b and permeability $k = \kappa^{-2}$, where κ^{-1} is the hydrodynamic penetration depth. The flow inside a shell of width $b - a$ is described by the Brinkman-Debye-Bueche equation,[15,16] and outside the particles by the Stokes equation.[36,37] The applied boundary conditions are that the fluid sticks to the core surface, and that the fluid velocity and stress change continuously across the outer surface of the shell. The particles are assumed to interact non-hydrodynamically by a hard-sphere no-overlap potential of radius b. The composite particle model is thus completely specified by the size ratio, $\gamma = a/b \leq 1$, the ratio, $y = \kappa b$, of the hard-sphere no-overlap interaction radius to the hydrodynamic penetration depth, and the particle volume fraction $\phi = (4/3)\pi n b^3$, where n is the number concentration of particles. Typical values for y in core-shell systems are in the range of 20–30.[2]

Using a precise hydrodynamic force multipole simulation method,[34,38] encoded in the HYDROMULTIPOLE program,[39,57] numerical results are presented for the high-frequency shear viscosity, η_∞, sedimentation coefficient, K, and the short-time translational and rotational self-diffusion coefficients, D_t and D_r. In our simulation method, the hydrodynamic particle structure enters only through the single-particle friction coefficients, which for our core-shell model are taken from Ref. 23. An additional advantage of our method is that higher order hydrodynamic multipoles are taken into account. This allows the calculation of transport coefficients with a strictly controlled precision to be made.

The purpose of the present work is to explore, with high precision, the dependence of short-time dynamic properties on concentration, relative core-to-particle size ratio, and shell permeability. We analyze the hydrodynamic influence of the core by quantifying the conditions for which the core-shell structure becomes noticeable in the short-time properties. The

simulation results span the full three-dimensional fluid-phase parameter space, with γ extending from 0 to 1, y from 10 to 100, and ϕ from 0.05 to 0.45. Each of the considered transport properties is discussed as a function of ϕ, for different values of y and γ. The numerical simulations in the limiting cases of $\gamma = 0$, corresponding to uniformly porous particles of radius b, and $\gamma = 1$ or $y = \infty$, corresponding to hard, non-permeable spheres of radius b, have been already performed and extensively analyzed in our previous publications.[40–45] In this work, the influence of the particle core is analyzed through comparison with simulation results for uniformly permeable spheres of the same radius b and the same value of y, corresponding to the limiting case $\gamma = 0$.

The paper is organized as follows. Section II describes the core-shell model. Furthermore, it includes a short description of the force multipole method and provides the expressions used in calculating the transport coefficients. The simulation results for the translational and rotational self-diffusion coefficients, sedimentation coefficient, and high-frequency viscosity for concentrated core-shell suspensions are presented in Section III. General trends in the behavior of the transport properties and the hydrodynamic influence of the core are discussed in Section IV. Our conclusions are contained in Section V. Appendix A includes the scattering coefficients for core-shell particles and describes the asymptotic analysis for the hydrodynamic influence of the dry core. Numerical tables giving the values of all calculated transport properties as functions of γ, y, and ϕ are contained in Appendix B. These tables should be useful to experimentalists and theoreticians alike dealing with the (hydro)dynamics of core-shell particles systems.

II. PARTICLE MODEL AND MANY-PARTICLE METHOD

A. Core-shell model

Our aim is to investigate generic permeability effects in concentrated dispersions of globular colloidal particles with a dry, solid core, and a permeable shell of arbitrary width. To minimize the number of system parameters, we use a simple core-shell particle model which disregards more specific shell properties such as a non-uniform permeability, compressibility, and related soft inter-particle direct interactions.

Following Masliyah *et al.*,[1] and Chen and Yeh,[22] we consider composite spheres consisting of a solid, solvent-impermeable core of radius a that is surrounded by an incompressible, uniformly permeable shell of width $b - a$ and constant permeability $k = \kappa^{-2}$, where κ^{-1} is the hydrodynamic penetration depth (see Fig. 1). We assume that the particles interact non-hydrodynamically only via a hard-sphere no-overlap pair potential of radius b.

The particles are dispersed in a Newtonian fluid of shear viscosity η_0. We describe the low-Reynolds number, incompressible solvent flow outside the composite spheres and inside their permeable shells by the Stokes[36,37] and Brinkman-Debye-Bueche[15,16] equations, respectively,

$$\eta_0 \nabla^2 \mathbf{v}(\mathbf{r}) - \eta_0 \kappa^2 \chi(\mathbf{r}) [\mathbf{v}(\mathbf{r}) - \mathbf{u}_i(\mathbf{r})] - \nabla p(\mathbf{r}) = 0. \quad (1)$$

Here, $\mathbf{v}$ and p are the velocity and pressure fields, respectively, of the incompressible Newtonian fluid. The characteristic function, $\chi(\mathbf{r})$, is equal to one for the field point $\mathbf{r}$ inside the shell of any of the particles, and zero outside the particles. The BDB equation describes the pore-size averaged flow inside a permeable shell. The shell skeleton of a particle i moves rigidly with the core centered at $\mathbf{R}_i$. Thus the skeleton velocity field inside the shell, $a < |\mathbf{r} - \mathbf{R}_i| < b$, of a particle i is given by

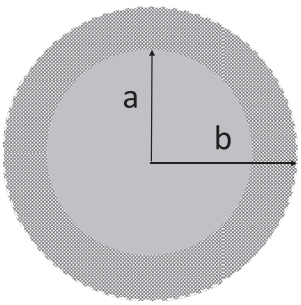

FIG. 1. Core-shell composite particle consisting of an impermeable (solid) core of radius a, covered by a uniformly permeable shell of width $b - a$ and hydrodynamic penetration depth κ^{-1}. Two particles interact directly by a hard-sphere no-overlap potential of radius b.

$$\mathbf{u}_i(\mathbf{r}) = \mathbf{U}_i + \boldsymbol{\omega}_i \times (\mathbf{r} - \mathbf{R}_i), \quad (2)$$

expressed in terms of the translational and rotational particle velocities $\mathbf{U}_i$ and $\boldsymbol{\omega}_i$, respectively.

Boundary conditions for the system of Eq. (1) are the following. The BDB equation inside the particle shells and the Stokes equation outside the particles are solved assuming that the solvent sticks to the core surfaces, i.e., $\mathbf{v}(\mathbf{r}) = \mathbf{u}_i(\mathbf{r})$ for $|\mathbf{r} - \mathbf{R}_i| = a$, and that the fluid velocity and stress change continuously across the outer spherical surfaces of the permeable shells, i.e., at $|\mathbf{r} - \mathbf{R}_i| = b$.

As noted in the Introduction, the model system of monodisperse core-shell particles is completely characterized by the three dimensionless parameters

$$\gamma = a/b, \quad (3)$$

$$y = \kappa b, \quad (4)$$

$$\phi = (4\pi/3) n b^3, \quad (5)$$

where n is the number concentration of particles, ϕ is the direct interaction volume fraction, and y expresses the outer radius in units of the hydrodynamic penetration depth. It would be a more natural choice to use, in place of y, the parameter $z = (b - a)\kappa$ which measures the shell width relative to the penetration depth. However, the parameter y has been used in related earlier work,[23] so we stick to its usage. Instead of $\{\gamma, y, \phi\}$ or $\{\gamma, z, \phi\}$, in following Zackrisson and Bergenholtz[21] one could equally well use the set $\{y = \kappa b, x = \kappa a, \phi\}$. Which of these sets is selected is just a matter of convenience since they can be straightforwardly expressed in terms of each other. An important point to note is that the BDB equation for the intra-shell flow applies only when the mean pore size of the shell skeleton is sufficiently smaller than the shell width, i.e., when $z = y(1 - \gamma)$ is sufficiently large.

For $\gamma = 1$, and also in the zero-penetration limit $y \to \infty$, non-permeable hard spheres of radius b are

described, whereas for $\gamma = 0$, uniformly permeable spheres of radius b are recovered. These limiting cases have been thoroughly analyzed over an extended concentration range in our previous publications.[40–45] The limiting case $\gamma = 0$ of uniformly permeable spheres is used in the present study as a reference to quantify the significance of the core. In the formal limit $y \to 0$, spherical annulus particles of no-overlap interaction radius b and hydrodynamic radius a are described. For a given value of $0 < \gamma < 1$, an annulus particle is qualitatively different from a core-shell particle since there is no hydrodynamic screening of the flow by a permeable shell. The annulus model can serve as an efficient model in numerous contexts, e.g., for spherical microgels with non-uniform density of segments, uniformly porous spheres,[43,44] or non-permeable charged colloidal spheres, where the outer radius b is interpreted as an effective excluded volume radius roughly accounting for the electrostatic repulsion. Short-time and long-time translational self-diffusion in the framework of the spherical annulus model has been discussed for dilute systems in Ref. 50, and for viscoelastic properties in Ref. 51. The spherical annulus model is of interest here only as a limiting case. Our major interest is in the hydrodynamic effects of the permeable shell and dry core on the short-time transport properties of concentrated systems.

B. Short-time transport properties

Using a hydrodynamic force multipole simulation method described in the following Sec. II C, we calculate transport properties for concentrated systems of core-shell particles characteristic of the colloidal short-time regime. On the short-time scale, the system is described by the equilibrium particle distribution. Numerical results are presented for the short-time translational and rotational self-diffusion coefficients, D_t and D_r, for the short-time sedimentation coefficient K, and for the high-frequency limiting shear viscosity η_∞ at low shear rates. For our core-shell particles model, these transport coefficients are functions of γ, y, and ϕ.

The short-time translational and rotational self-diffusion coefficients of a quiescent, isotropic system are given in frame-invariant notation by[39,52]

$$D_t = \frac{k_B T}{3} \mathrm{Tr} \left\langle \frac{1}{N} \sum_{i=1}^{N} \boldsymbol{\mu}_{ii}^{tt}(\mathbf{X}) \right\rangle, \tag{6}$$

$$D_r = \frac{k_B T}{3} \mathrm{Tr} \left\langle \frac{1}{N} \sum_{i=1}^{N} \boldsymbol{\mu}_{ii}^{rr}(\mathbf{X}) \right\rangle, \tag{7}$$

where $\mathbf{X} = \{\mathbf{R}_1, \ldots, \mathbf{R}_N\}$ is the configuration of $N \gg 1$ sphere centers, and Tr denotes the trace operation. The second-rank hydrodynamic mobility tensor, $\boldsymbol{\mu}_{ii}^{tt}(\mathbf{X})$, linearly relates the force acting on a particle i to its translational velocity, for zero forces and torques exerted on the other particles. Likewise, the second-rank tensor $\boldsymbol{\mu}_{ii}^{rr}(\mathbf{X})$ relates the torque acting on a particle i to its rotational velocity. For the present core-shell model system, the average $\langle \cdots \rangle$ is taken over an equilibrium distribution of spheres of radius b (i.e., with the same probability for all non-overlapping configurations of spheres), consistent with the periodic boundary conditions used in our simulations.

The statistical mechanical definition of the short-time sedimentation coefficient K in a homogeneous suspension of spherical particles subject to a weak and uniform force field is given by[53,54]

$$K = \frac{U}{U_0} = \frac{k_B T}{3 D_0^t} \mathrm{Tr} \left\langle \frac{1}{N} \sum_{i,j=1}^{N} \boldsymbol{\mu}_{ij}^{tt}(\mathbf{X}) \right\rangle_{\mathrm{irr}}. \tag{8}$$

According to this equation, K is equal to the modulus U of the short-time mean sedimentation velocity of monodisperse particles which points into the direction of the force field of strength F, divided by the sedimentation velocity, $U_0 = (D_0^t / k_B T) F$, of an isolated particle of radius b in the same force field. The single-particle translational diffusion coefficient, $D_0^t = D_t(\gamma, y, \phi = 0)$, depends on the parameters of the underlying hydrodynamic particle model. Equation (8) for K involves the long-range distinct translational mobilities $\boldsymbol{\mu}_{ij}^{tt}$ (with $i \neq j$), in addition to the shorter range self-mobilities $\boldsymbol{\mu}_{ii}^{tt}$ appearing also in the expressions for D_t and D_r. Therefore, to obtain the correct finite value for U, the average is taken with respect to the regularized, irreducible part of the mobility tensors, without long-distance contributions. In Eq. (8), this is indicated by the subscript at the average symbol. The average can be alternatively taken over a periodic cubic cell of size $\mathcal{L}$, in the limit of $\mathcal{L} \to \infty$. It can be shown that K is equal to the zero-wavenumber limit of the so-called hydrodynamic function $H(q)$ which can be determined by scattering experiments as a function of the wavenumber q. A detailed discussion of $H(q)$ for uniformly permeable spheres has been given in Refs. 40 and 41.

The high-frequency viscosity linearly relates the average deviatoric suspension stress in an isotropic system to the applied high-frequency oscillatory rate of strain. In the linear response regime of low shear considered here, η_∞ is determined by the equilibrium particle distribution of the non-sheared system. The statistical mechanical expression for η_∞ is[55]

$$\eta_\infty = \eta_0 + \frac{1}{10V} \left\langle \sum_{i,j=1}^{N} \boldsymbol{\mu}_{ij,\alpha\beta\beta\alpha}^{dd} \right\rangle_{\mathrm{irr}}. \tag{9}$$

The Cartesian components of the $3 \times 3 \times 3 \times 3$ dipole-dipole mobility matrix $\boldsymbol{\mu}_{ij}^{dd}$ linearly relate the rate of strain applied to sphere j to the symmetric hydrodynamic force dipole moments acting on the surface of sphere i. The Einstein summation convention for the Cartesian indices α and β is implied. The regularized average $\langle \cdots \rangle_{\mathrm{irr}}$ can be taken in general over an arbitrary ensemble of random configurations of non-overlapping particles, consistent with the periodic boundary conditions. In the linear response regime considered here, equilibrium configurations of N spheres in the basic simulation cell of volume $V = \mathcal{L}^3$ are used for systems in an isotropic fluid state.

It should be noted that in the present core-shell model, η_∞ is influenced by the excluded volume interactions through the equilibrium averaging only. The high-frequency viscosity should be distinguished from the static or zero-frequency viscosity, $\eta = \eta_\infty + \Delta\eta$, which has an additional positive-valued contribution, $\Delta\eta$, arising from the time-integrated shear stress correlation relaxations. The relaxation term $\Delta\eta$ depends both

on direct and hydrodynamic interactions. For concentrated systems, it is substantially larger than η_∞.

In our numerical calculations of transport properties based on Eqs. (6)–(9), extrapolations to the thermodynamic limit $N \to \infty$ (with $n = N/V$ kept constant) are included. The self-mobility and distinct mobility tensors $\boldsymbol{\mu}_{ij}^{tt}$, $\boldsymbol{\mu}_{ij}^{rr}$, and $\boldsymbol{\mu}_{ij}^{dd}$ are evaluated from the force multipole expansion method discussed in the following Sec. II C. The mobility tensors depend on the configuration of all particles in the system, and on the hydrodynamic particle model.

Results for D_t, D_r, and U are presented in non-dimensionalized form by dividing these quantities by their respective values for single particles, and η_∞ is normalized by the solvent viscosity η_0. The diffusion and rheology in highly diluted suspensions of uncorrelated core-shell particles are characterized by the single-particle translational and rotational diffusion coefficients $D_0^t(\gamma, y)$ and $D_0^r(\gamma, y)$, and the intrinsic viscosity $[\eta](\gamma, y)$. The latter is a single-particle property defined by the leading-order virial expansion,[56]

$$\eta_\infty = \eta_0(1 + [\eta]\phi + \mathcal{O}(\phi^2)), \tag{10}$$

for the (high-frequency) viscosity.

As we have noted in the Introduction, the single-particle coefficients are known analytically for the core-shell particle model. They can be expressed as[23]

$$D_0^t(\gamma, y) = k_B T \mu_0^t(\gamma, y) = \frac{k_B T}{4\pi\eta_0 A_{10}(\gamma, y)}, \tag{11}$$

$$D_0^r(\gamma, y) = k_B T \mu_0^r(\gamma, y) = \frac{k_B T}{8\pi\eta_0 A_{11}(\gamma, y)}, \tag{12}$$

$$[\eta](\gamma, y) = \frac{3}{8\pi\eta_0 b^3}\mu_0^d(\gamma, y) = \frac{A_{20}(\gamma, y)}{b^3}. \tag{13}$$

Here $\mu_0^t(\gamma, y)$, $\mu_0^r(\gamma, y)$, and $\mu_0^d(\gamma, y)$ denote the corresponding single core-shell particle translational, rotational and dipole mobility coefficients, which in turn are determined by the scattering coefficients A_{10}, A_{11}, and A_{20} given explicitly in Appendix A.[68] The core-shell diffusion coefficients D_0^t, D_0^r attain their minimal values, and $[\eta]$ its maximal value for non-permeable hard spheres of radius b (what corresponds to zero shell permeability or equivalently, zero shell width), where $A_{10} = 3b/2$, $A_{11} = b^3$, and $A_{20} = 5b^3/2$. The single-particle diffusion coefficients become larger, and the intrinsic viscosity smaller, with increasing permeability (i.e., decreasing κ), and increasing shell width.

Regarding Eqs. (11)–(13) for the single-particle properties of a composite sphere of arbitrary spherical shell width, we note that Masliyah *et al.*[1] have provided the first derivation of an analytic expression for $D_0^t(\gamma, y)$, using the stream function formulation. They also discuss in detail the various limiting cases of their expression. Veerapaneni and Wiesner[25] have extended the stream function formulation to obtain the translational diffusion coefficient of a multi-layered sphere, used as a model for a fractal aggregate of radially varying permeability (see also Ref. 24). While the intrinsic viscosity of core-shell spheres was examined earlier by Chen and Ye[22] on a more numerical basis, an explicitly analytical result for $[\eta](\gamma, y)$ was first derived, and discussed in great detail, by Zackrisson and Bergenholtz.[21] Chen and Ye[22] also derived explicit numerical results for the single-particle rotational and translational diffusion coefficients $D_0^r(\gamma, y)$ and $D_0^t(\gamma, y)$ as functions of (reduced) shell permeability and γ. In addition, they examined the Faxén theorems for the hydrodynamic translational force, torque and symmetric force dipole on a core-shell sphere when an arbitrary flow field is imposed. Recently, all the scattering coefficients for core-shell particles have been derived,[23] what allows for precise computations of the self-diffusion, sedimentation and viscosity coefficients of concentrated core-shell suspensions.

C. Many-particle method

The theoretical algorithm used in this work to account for the non-pairwise additive HIs between core-shell composite spheres is based on solving the Stokes equations by a multipole expansion method. For suspensions of core-shell particles, this method is essentially the same as the procedure applied in Ref. 40 to systems of uniformly permeable particles, only the single-particle friction operator has a different form. Therefore, we can be brief in our explanation of the method.

In a nutshell, the multipole method is as follows: For a multipolar description of the HIs between N suspended particles, the fluid flow problem is formulated in the induced force picture,[46–48] where the presence of the particles immersed in the fluid is accounted for by a density, $\mathbf{f}_i(\mathbf{r})$, of forces exerted by a particle i on the fluid. The force density is introduced as a source term in the right-hand side of the Stokes equations (1) according to

$$\eta\nabla^2\mathbf{v} - \nabla p = -\sum_{i=1}^{N}\mathbf{f}_i(\mathbf{r}), \quad \nabla\cdot\mathbf{v} = 0. \tag{14}$$

In an unbounded suspension in presence of an ambient flow field, $\mathbf{v}_0$, created by external sources in the absence of particles, the local velocity field, $\mathbf{u}_i$, of a translating and rotating particle i satisfies inside the particle the relation,

$$\mathbf{u}_i - \mathbf{v}_0 = \sum_{j\neq i}^{N}\mathbf{G}(ij)\mathbf{f}_j + \mathbf{Z}_0^{-1}(i)\mathbf{f}_i, \tag{15}$$

for $i = 1, \ldots, N$. The first contribution on the right-hand side of Eq. (15) does not depend on a hydrodynamic particle model. Here, $\mathbf{G}(ij)$ is an abbreviated notation for the integral Green operator for an unbounded fluid, with the Oseen tensor $\mathbf{T}_0$ as its kernel,[36,37,57] describing the velocity field incident on particle i, and induced by the force density on another particle j.

The second term on the right-hand side of Eq. (15) describes the velocity contribution to particle i originating from the induced force density located within the same particle i. This contribution is described in terms of the inverse one-particle friction operator, $\mathbf{Z}_0^{-1}(i)$, and it does depend on the hydrodynamic particle model. For core-shell particles, it is thus different in general from the velocity contribution to uniformly permeable spheres.

If a single particle i, whose core and permeable shell skeleton is translating and rotating according to the local velocity field $\mathbf{u}_i$ specified in Eq. (2), is immersed in an incident fluid flow field $\mathbf{v}^{in}$, it will resist the flow by exerting on the

fluid a force density $\mathbf{f}_i$, with

$$\mathbf{f}_i = \mathbf{Z}_0(i)\,(\mathbf{u}_i - \mathbf{v}^{in}), \tag{16}$$

which depends linearly on $\mathbf{v}^{in} - \mathbf{u}_i$.

Equation (15) is solved for the induced force densities by truncating the resulting multiple scattering series, and inverting the matrix $\mathbf{G} + \mathbf{Z}_0^{-1}$. Next, the grand friction matrix, $(\mathbf{G} + \mathbf{Z}_0^{-1})^{-1}$, is inverted in the space spanned by the lower spherical multipole functions, to evaluate the mobility coefficients. The details of the described multipole method can be found, e.g., in Ref. 40.

We emphasize that the single-particle operator, $\mathbf{Z}_0$, is the only object that must be changed when different hydrodynamic models for the particle interior and the boundary conditions at its surface are considered. The basic Eq. (15) remains the same, and so does the operator $\mathbf{G}$ which, as the propagator of the HIs, depends only on the properties of the suspending fluid and its outer boundaries.

The single-particle operator, $\mathbf{Z}_0$, is evaluated in terms of the scattering coefficients $A_{l\sigma}(\gamma, y)$ and $B_{l2}(\gamma, y)$, with $l = 1, 2, 3, \ldots$ and $\sigma = 0, 1, 2$ (see Ref. 34 for details). For core-shell particles, the scattering coefficients $A_{l\sigma}(\gamma, y)$ and $B_{l2}(\gamma, y)$ for all values of l and σ have been evaluated by Cichocki and Felderhof in Ref. 23 and are listed, for convenience and later use in an asymptotic analysis, in Appendix A.

In our numerical calculations of the short-time transport properties of core-shell particles, a periodically replicated cubic simulation box including N particles has been used. For such a periodic system, the main structure of the multipole method remains the same as the one for the unbounded fluid described above. The only difference is that, for $i \neq j$, the Green integral operator $\mathbf{G}(ij)$ has now the periodic Hasimoto tensor, $\mathbf{T}_H$,[49] as its kernel. In addition, there appears now a self-part Green operator, $\mathbf{G}(ii)$, with $\mathbf{T}_H$–$\mathbf{T}_0$ as its kernel, which accounts for flow propagation due to all the periodic images.[39] The details can be found in Ref. 40.

D. Numerical calculations

Numerical computations of the short-time translational and rotational self-diffusion coefficients, high-frequency effective viscosity, and sedimentation coefficient have been performed in following way: The multipole method outlined in the previous section has been has been implemented in the numerical package HYDROMULTIPOLE.[38,39,57] In the computations performed in this paper, the core-shell scattering coefficients from Ref. 23, listed in Appendix A, have been used. Cubic periodic boundary conditions have been imposed, with $N = 256$ particles in the periodically replicated cell.

The short-time transport properties have been evaluated by averaging over 150–250 independent random particle configurations, for each considered parameter set $\{\gamma, y, \phi\}$. In general, for the volume fractions $\phi = 0.05$, 0.15, and 0.25, averages were obtained from 250 particle configurations. For higher volume fractions ($\phi = 0.35$ and 0.45) 150 configurations were used. The number of the random configurations in the calculated transport properties was adjusted to reach the relative accuracy of the order of 1% or better. Such a precision was obtained owing to two additional procedures, described below.

The multipole truncation parameter value $L = 3$ has been used. To obtain high precision data extrapolation to larger values of L are needed. For strongly permeable porous layer ($y \leq 20$ and annulus model) results were extrapolated from $L = 3$ to $L = 6$. For $y = 50$ and 100 extrapolations were performed from $L = 3$ to $L = 8$.

Extrapolation to the thermodynamic limit $N \to \infty$ has been performed for the sedimentation and translational self-diffusion coefficients as described in Ref. 40. The high-frequency effective viscosity and the rotational self-diffusion coefficient have been excluded from this finite-size correction procedure since they are not critically dependent on system size.

Concluding, taking into account the N- and L-extrapolations and the averaging over initial configurations, the relative accuracy in the calculated transport properties is of the order of 1% or better for the sedimentation coefficient, and 0.5% or better for the translational and rotational self-diffusion coefficients and the effective viscosity.

III. RESULTS FOR MANY-PARTICLE SYSTEMS

Using our multipole simulation method encoded in the HYDROMULTIPOLE program package, we have evaluated the short-time translational and rotational self-diffusion coefficients D_t and D_r, the sedimentation coefficient K, and the high-frequency effective viscosity η_∞ of a suspension of core-shell particles, normalized by their respective zero concentration values. The results for the four transport properties are presented and discussed in the order stated above. Our simulation study covers essentially the complete three-parametric fluid-phase regime of the model system, with different volume fractions up to $\phi = 0.45$, and the whole range of core-to-particle size ratios, $\gamma = a/b$, from zero (uniformly permeable spheres of radius b) up to one (non-permeable spheres of radius b). The particle radius to hydrodynamic penetration depth ratio, $y = \kappa b$, has been varied from 0 (spherical annulus particles) over 10 (strongly permeable shell) up to 100. The endmost value of y characterizes core-shell particles with an only slightly permeable shell. Corresponding simulation results for the limiting case, $y = \infty$, of non-permeable hard spheres with stick boundary conditions have been presented already in earlier work (see, e.g., Refs. 12 and 61–67), and are now recalculated and shown in all the plots as the equivalent limit of $\gamma = 1$.

Figures 2–5 in Secs. III–IV illustrate that even if particle shells are hardly permeable (e.g., $y = 100$) and very thin (e.g., $\gamma = 0.97$), still the transport properties of concentrated core-shell systems cannot be accurately approximated by an impermeable hard-sphere model. (The thin-shell limit will be discussed in a separate paper.) Moreover, for concentrated systems of core-shell particles with a large shell permeability, values of the transport coefficients depend significantly on the core size, with variations even by a factor of 2. Compare, e.g., uniformly permeable particles ($\gamma = 0$, no core) with impermeable hard spheres ($\gamma = 1$, no shell) of the same size, for $\phi = 0.45$ and $y = 10$. The

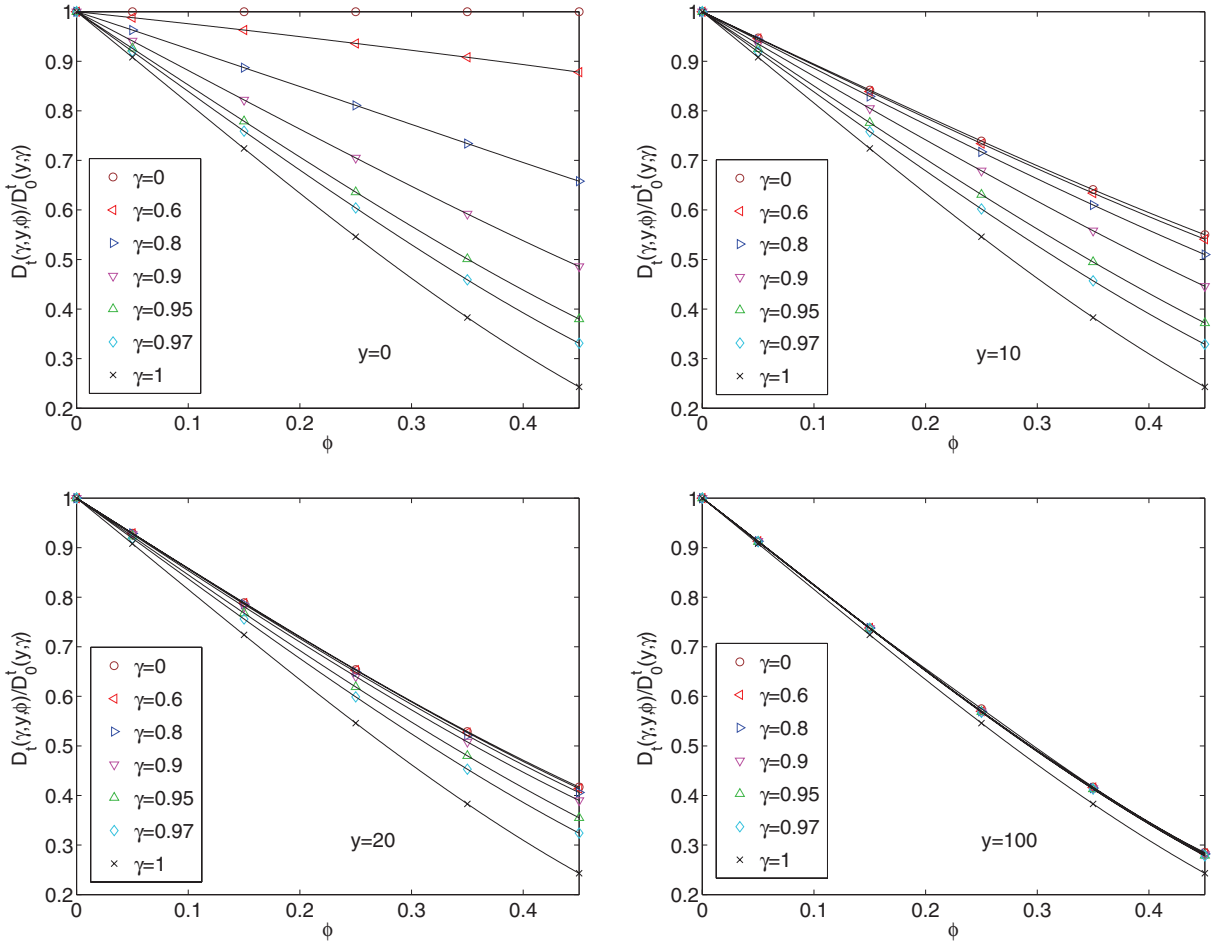

FIG. 2. Normalized translational self-diffusion coefficient, $D_t(\gamma, y, \phi)/D_0^t(\gamma, y)$, of core-shell particles as a function of ϕ, for various core-to-particle size ratios, $\gamma = a/b$, as indicated in the panel legends. The four panels are ordered with respect to the size-to-penetration depth ratio, $y = \kappa b$, with values from $y = 0$ (spherical annulus particles) to $y = 100$ (only slightly permeable shell). Symbols: HYDROMULTIPOLE simulation results continuously connected by splines.

precise numerical values for the transport coefficients are listed in Appendix B.

A. Translational and rotational self-diffusion

Our simulation results for the reduced short-time translational and rotational self-diffusion coefficients of core-shell particles, $D_t(\gamma, y, \phi)$ and $D_r(\gamma, y, \phi)$, non-dimensionalized by the respective single-particle (i.e., infinite dilution) coefficients $D_0^t(\gamma, y)$ and $D_0^r(\gamma, y)$ given in Eqs. (11) and (12), are depicted as functions of the volume fraction ϕ in Figs. 2 and 3, respectively. The division by the infinite dilution values makes the effect of the solvent-mediated inter-particle HIs on these quantities more transparent. Four different values, $y = 0$, 10, 20, and 100, of the particle size-to-penetration depth ratio, $y = \kappa b$, are shown.

The special case $y = 0$ is a singular limit which describes annulus particles of hard-sphere no-overlap interaction radius b where the fluid can reach the hydrodynamic particle surface of radius $a < b$ without any screening. The spherical annulus model is very useful as a minimal hydrodynamic model for many systems of particles, such as, e.g., permeable particles with a large gradient of the segment concentration, non-permeable particles with long-range (non-steric) repulsion, such as charge-stabilized particles at low salinity, or even uniformly porous particles of the hydrodynamic radius modeled as a hard-core radius.[43,44] The explored core-to-particle size ratio, $\gamma = a/b$, is varied in our simulations from 0 (uniformly permeable sphere of radius b with no dry core) over 0.6 (thick permeable shell) to 1 (hard sphere of radius b with no permeable shell).

Consider first the simulation data (symbols) for D_t/D_0^t depicted in Fig. 2. The numerical values are listed in the left panel of Table I in Appendix B. The simulation data in this figure, and in the following ones, are connected continuously by splines to guide the eye. All depicted curves for D_t/D_0^t are convex functions, which decrease monotonically with increasing volume fraction ϕ. The decrease is approximately linear for $\phi \lesssim 0.3$, with a slight upward curvature visible at larger concentrations. The decrease of D_t/D_0^t with increasing ϕ is as a consequence of the increasing HIs between neighboring particles, which tend to slow both the translational and rotational self-diffusion. A non-zero shell permeability has the general effect of weakening the HIs, for the reason that the fluid can penetrate (flow through) the particle shell. The attenuation of the HIs, in turn, gives rise to an enlarged D_t/D_0^t. For a given core-to-particle size ratio $\gamma = a/b$, this enlargement is more pronounced for a larger

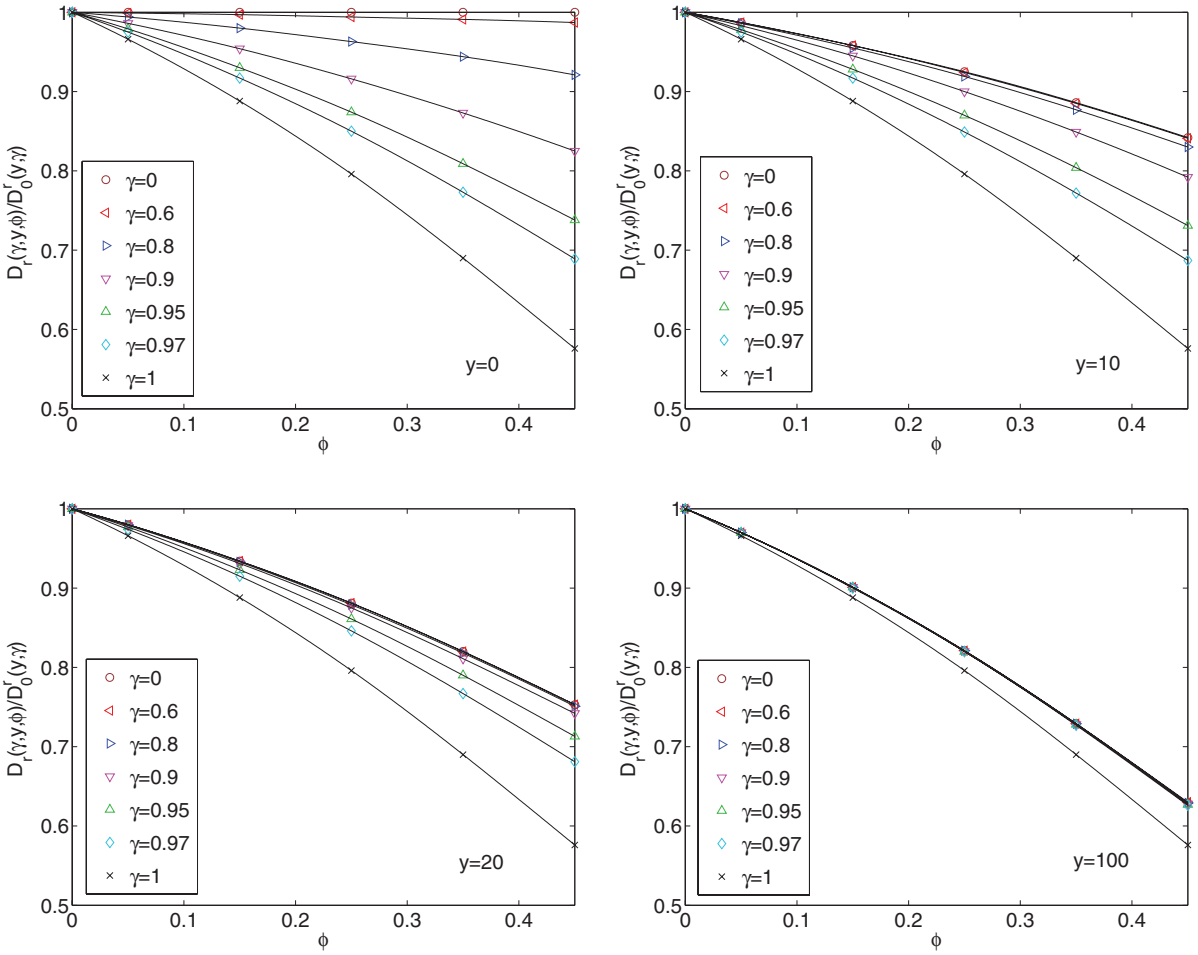

FIG. 3. Normalized rotational self-diffusion coefficient $D_r(\gamma, y, \phi)/D_0^r(\gamma, y)$. Values of the parameters and notation are the same as in Fig. 2.

shell permeability, i.e., a smaller value of y. This can be noticed in Fig. 2 by comparing iso-γ curves at different values of y. The first panel corresponds to the annulus limit $y = 0$. The upper limiting curves in the four panels are reached in the uniformly permeable sphere limit, $\gamma = 0$, when there is no core.

The attenuating effect of the shell permeability on the HIs is counteracted by the dry core surfaces to which the fluid sticks. In the limiting case, $\gamma = 1$, of non-permeable, uniform spheres of radius b with stick surface boundary conditions, there is no shell left which can weaken the HIs. Therefore, D_t/D_0^t attains for $\gamma = 1$ its lowest value, at a given ϕ, which is independent of y. Notice in this respect the $\gamma = 1$ curves in the four panels of Fig. 2, which are all identical. With decreasing γ, i.e., increasing shell width $b - a$, the slowing hydrodynamic influence of the cores lessens, and the $D_t/D_0^t(\phi)$ curves shift upwards to larger values. The large-shell-width curves for $\gamma \leq 0.6$ are very close to the curve for $\gamma = 0$.

The last remark related to the upshift is the following. In Fig. 2, it is remarkable that the $\gamma = 1$ curve, which corresponds to the hard non-permeable sphere, is well separated from all the other curves, even those describing a core-shell particle with a very thin hardly permeable shell at $\gamma = 0.97$ and $y = 100$. Therefore, there exist a relatively large, measurable difference between values of the self-diffusion coefficient for hard non-permeable spheres and core-shell particles of the same outer radius and a very thin, weakly permeable shell. This effect is caused by incompressibility of the fluid in the thin gap between two near-by particle outer surfaces. For non-permeable particles, the hydrodynamic resistance caused by the relative motion of two near-by particle boundaries blows up to infinity when the gap size tends to zero. However, such a lubrication singularity does not appear if the fluid can flow into the particle, even when there is only a very narrow and weakly permeable outer shell. Therefore, the lubrication interactions are very strong between hard non-permeable spheres, but much weaker between core-shell particles, even for extremely thin and only slightly permeable outer shells. This difference is important, because averaging over configurations with close-by particles, interacting through the lubrication layer, gives a significant contribution to the translational self-diffusion coefficient. A similar effect is observed for the rotational self-diffusion coefficient and the effective viscosity.

The present discussion of D_t/D_0^t applies basically also to the reduced rotational self-diffusion coefficient. The simulation results for D_r/D_0^r are listed in the right panel of Table I in Appendix B, and plotted in Fig. 3 as a function of ϕ, for values of γ and y as in Fig. 2. The most significant difference to translational self-diffusion is the

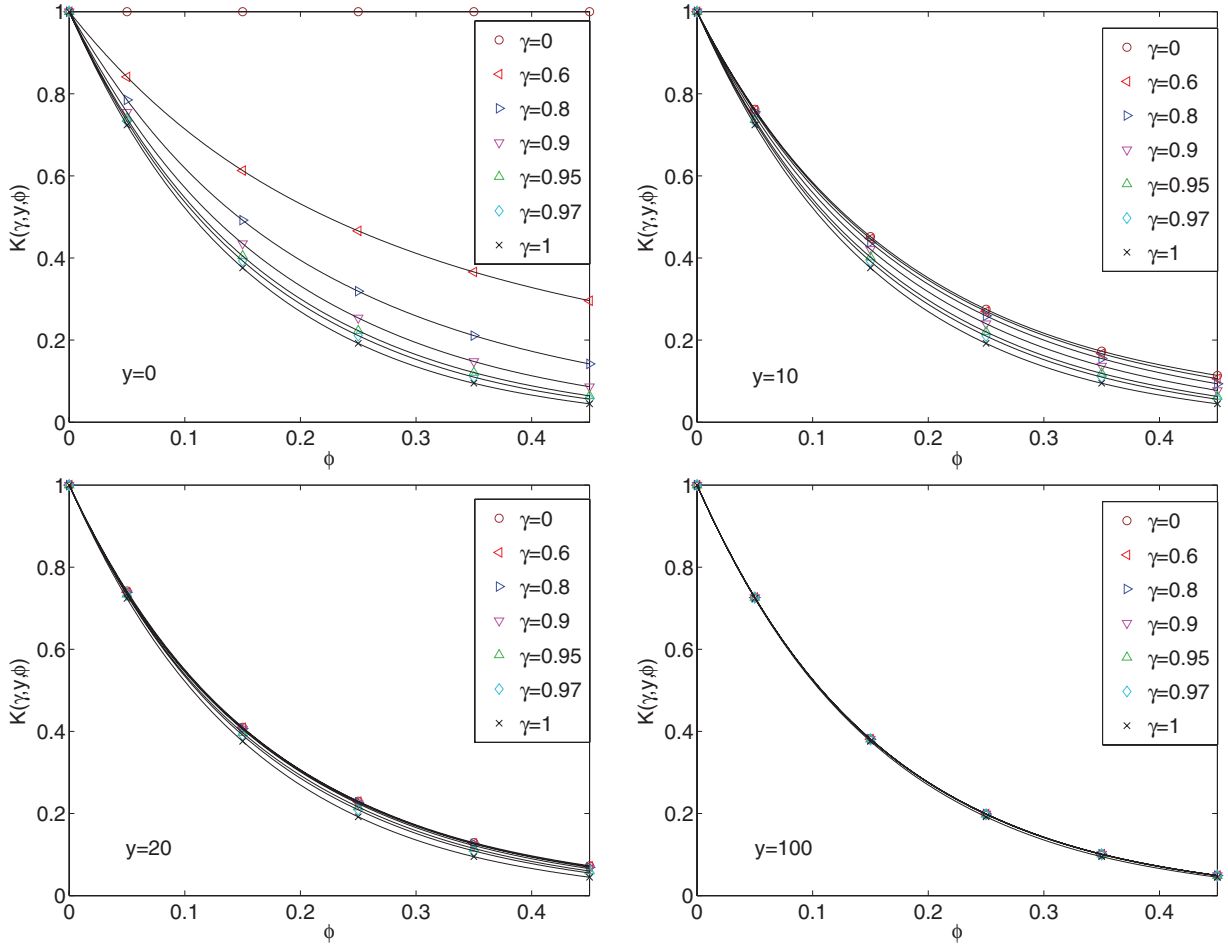

FIG. 4. Sedimentation coefficient $K(\gamma, y, \phi)$. Values of the parameters and notation are the same as in Fig. 2.

distinctly concave shape for most of the D_r curves, and the smaller deviation of the rotational diffusion coefficient from its infinite dilution value for a given ϕ. Note here the different ordinate scales in Figs. 2 and 3. The slowing effect of the HIs is clearly weaker for rotational self-diffusion. On a qualitative level, we can explain this by the different flow characteristics of the two self-diffusion mechanism: The hydrodynamic self-mobility associated with a tracer particle translating towards a second (caging) one decays as $1/r^4$ at large separation, r, of two particles. The corresponding self-mobility of a tracer particle in rotational motion relative to a second one decays much faster at long distances, according to $1/r^6$, leading thus to a weaker hydrodynamic coupling of particle pairs.

B. Sedimentation coefficient

As explained in Sec. II B, the (short-time) sedimentation coefficient, $K = U/U_0$, is equal to the mean sedimentation velocity, U, of a weakly settling, homogeneous suspension of monodisperse particles, measured in units of its zero concentration limiting value U_0.

In Fig. 4, the sedimentation coefficient of core-shell particles is displayed as a function of ϕ, for the same values of y and γ as in the preceding two figures. The simulation values of K are summarized in the left panel of Table II in Appendix B.

Sedimentation is qualitatively different from translational self-diffusion where a tagged particle is thermodynamically driven, in a squeezing motion, towards another particle in front of it. In sedimentation, all particles and not just a single one are forced to move on the average in the direction of a weak external force field (in the linear response regime considered in this work), with the distinct mobility coefficient scaling as the inverse interparticle distance. The cooperative particle motion sets up a uniform fluid backflow, created by a pressure gradient directed along the direction of the external force field, which balances the non-zero, buoyancy-corrected total external force on the particles. The laminar friction between back-flowing fluid (the latter not present in self-diffusion at any ϕ) and the settling particles strongly reduces K at larger volume fractions. This reduction of K is more pronounced than in translational self-diffusion (see here the different scales of the ordinate axes of Figures 2 and 4).

The most striking difference in the concentration dependence of K relative to those of the two self-diffusion coefficients, which can be clearly noticed from Fig. 4, is the small sensitivity of the sedimentation coefficient on the shell width (values of γ), even at non-small permeabilities. For $y \gtrsim 20$, the concentration curves of K form a narrow bundle for the whole range of shell widths. For $y = 20$, the absolute width of the bundle is apparently small, but the relative differences still

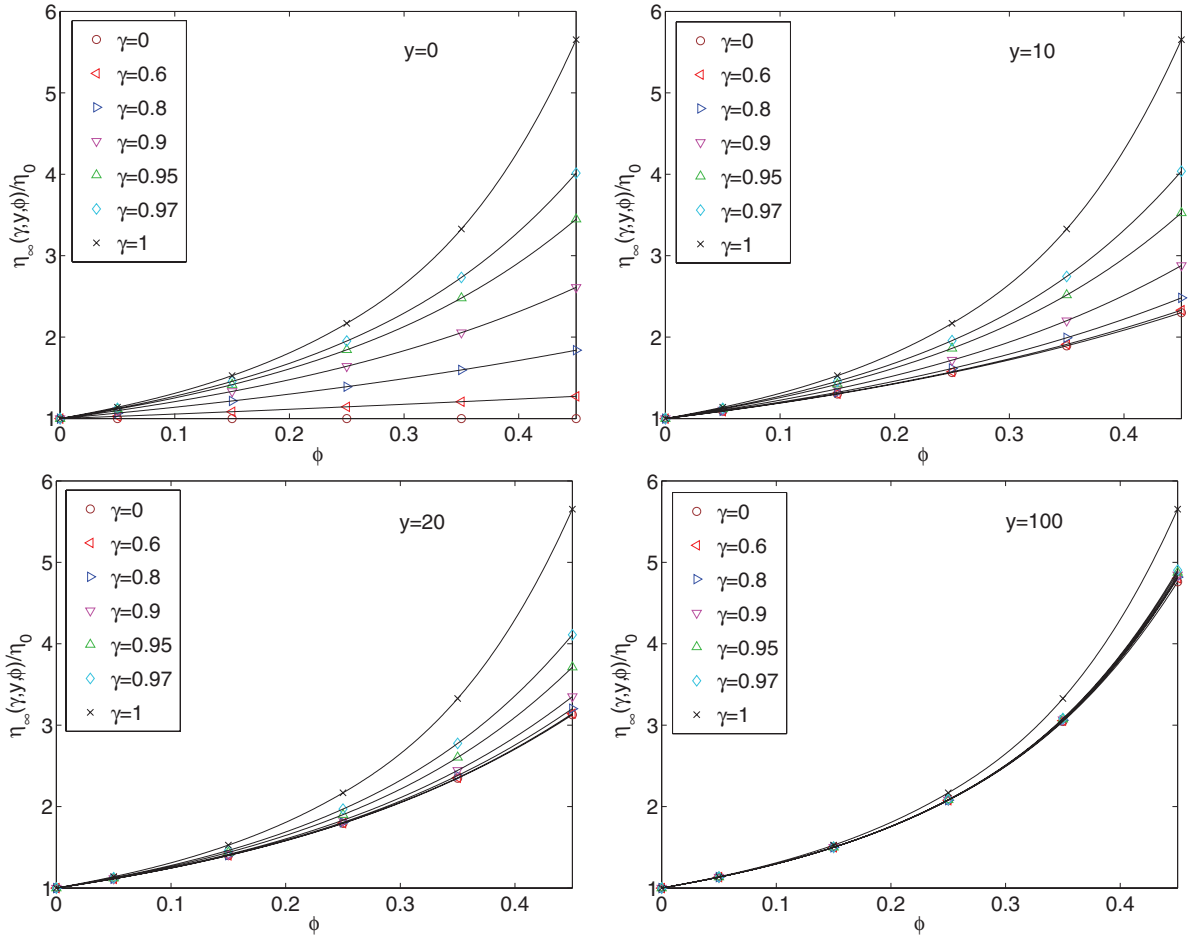

FIG. 5. Normalized high-frequency viscosity, $\eta_\infty(\gamma, y, \phi)/\eta_0$. Values of the parameters and notation are the same as in Fig. 2.

remain significant, owing to a very small sedimentation velocity at large concentrations, and the large sensitivity of the sedimentation coefficient to changes of volume fraction at small and moderate concentrations. However, for a larger value $y = 100$, the bundle becomes really very thin, and even the relative differences become irrelevant. The flow pattern inside the permeable shells has only a small effect on the reduced common settling velocity of uniformly distributed monodisperse particles.

For the sedimentation coefficient, unlike for other transport coefficients, the curve corresponding to hard non-permeable spheres ($\gamma = 1$) practically does not differ from those corresponding to core-shell particles with a thin slightly permeable shell ($\gamma = 0.97$ and $y = 100$).

C. High-frequency viscosity

Our results for the reduced high-frequency viscosity, $\eta_\infty(\gamma, y, \phi)/\eta_0$, are shown in Fig. 5 and tabulated in the right panel of Table II in Appendix B. The high-frequency viscosity, associated with the built-up of hydrodynamic stresslets (symmetric force dipoles) caused by force- and torque-free spheres in weak shear flow, increases with increasing volume fraction. In line with our earlier discussion on the effect of permeability, the increase of η_∞ is most pronounced for zero shell width ($\gamma = 1$).

Like for self-diffusion, but different from sedimentation, for $y \sim 20$ there is a pronounced increase in the viscosity curves with decreasing shell width (increasing γ). For low permeability ($y = 100$) where the penetration length is only one percent of the particle radius, the viscosity increases with γ significantly only when the shrinking shell width becomes comparable to the hydrodynamic penetration length, giving rise to the curve bundles at lower γ visible in the panels for $y = 20$ and 100.

IV. INFLUENCE OF THE CORE

In this section, we explore the hydrodynamic influence of the core, by comparing the transport properties of core-shell particles with those of uniformly permeable spheres ($\gamma = 0$) of equal, fixed radius b, equal permeability (i.e., equal y) and equal volume fraction ϕ, defined by Eq. (5). For this purpose, we calculate, and plot in Fig. 6, the relative differences,

$$\Delta f(\gamma, y, \phi) = \left| \frac{f(\gamma, y, \phi) - f(0, y, \phi)}{f(0, y, \phi)} \right|, \qquad (17)$$

for $f = D_t/D_0^t$, D_r/D_0^r, $K = U/U_0$ and η_∞/η_0, and analyze them as functions of the core-to-particle size ratio γ, for fixed values of y and ϕ.

We investigate the concentration dependence of the core influence, by comparing the suspension at $\phi = 0.45$ with a system of isolated core-shell particles. For the latter, the

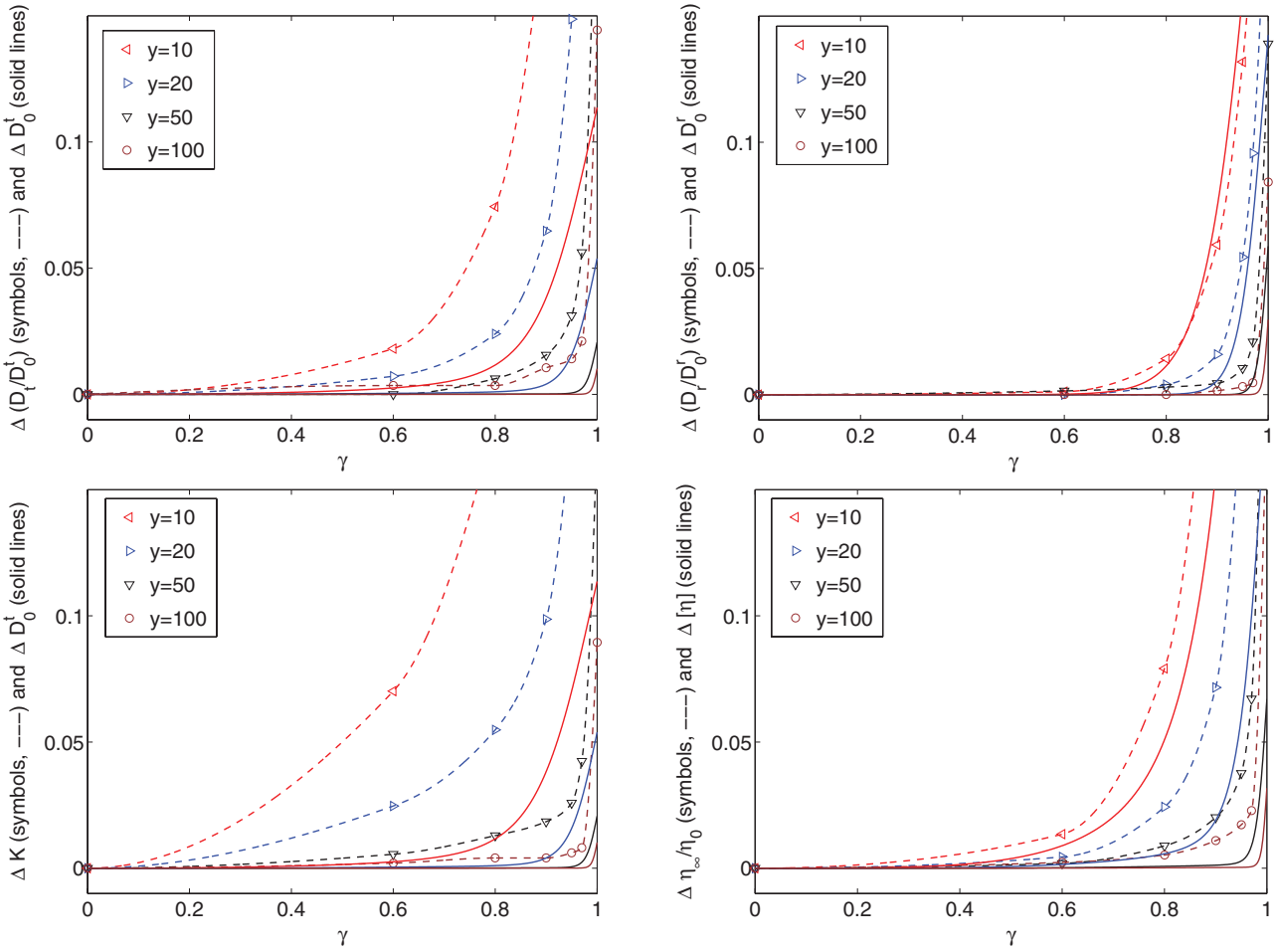

FIG. 6. The relative difference, see Eq. (17), between the core-shell and the uniformly permeable particle transport coefficients, as functions of the ratio, γ, of the core-to-particle radius, for the rotational and translational self-diffusion coefficients, sedimentation coefficient and high-frequency viscosity. Different colors correspond to different values of y. Symbols connected by dashed splines denote simulation results for $\phi = 0.45$. Solid lines describe isolated particles.

relative differences between the core-shell and permeable particle coefficients with the same permeability and radius, are defined by Eq. (17) with $f = D_0^t$, D_0^r, and $[\eta]$. These quantities are analytically calculated using Eqs. (11)–(13) and (A14)–(A16), and plotted in Fig. 6.

For the system of isolated particles (solid lines in Fig. 6), the essential observation is that, even for a highly permeable shell, the core influence is practically invisible even for a relatively large solid core. For example, the relative difference between core-shell and uniformly permeable particles is smaller than 1% if $\gamma \lesssim 0.6 - 0.8$ and $y = 10$, and in a wider range of γ for less permeable shells (larger values of y).

We now use the tables in Appendix B to evaluate the relative differences, Δf, at $\phi = 0.45$. The results are depicted in Fig. 6, where symbols corresponding to the simulation points are linked by dashed splines. We emphasize that the plots in Fig. 6 are meaningful owing to the extremely high precision of our results.

For the rotational self-diffusion, the relative differences at $\phi = 0.45$ are quite close to those for a system of isolated particles, However, for the translational diffusion and high-frequency viscosity, the influence of the core increases with the concentration, and in case of sedimentation, the influence of the core is far more significant at large concentrations than for dilute systems of particles non-interacting hydrodynamically with each other, in particular for shells with higher permeability. This effect is explained by the significant $1/r$ long-distance hydrodynamical mobility contributions modified by the interparticle correlations.[53]

We extract an important criterion, which states that the hydrodynamic influence of the core on short-time transport properties is practically negligible for $\kappa(b-a) \gtrsim 5$, i.e., when the penetration depth is less than about one fifth of the shell width. In this case, even concentrated suspensions can be considered as suspensions of uniformly permeable spheres of permeability equal to that of the shell.

We will now justify the core criterion theoretically. Having analytic expressions for all the scattering coefficients in Eqs. (A1)–(A4), we discuss their generic dependence on γ and y, and therefore, at the same time, the generic dependence on γ and y of the transport coefficients of concentrated suspensions. We will do this explicitly for the example of $A_{l0}(\gamma, y)$; the same conclusions are easily derived for all the other scattering coefficients. We will determine how well the core-shell value, $A_{l0}(\gamma, y)$, is approximated by the corresponding value, $A_{l0}(0, y)$, for a uniformly permeable sphere.

The BDB equations for the average flow inside a uniformly permeable shell apply when the shell width is comparatively large compared to the hydrodynamic penetration depth, i.e., when $y - x$ is significantly larger than unity. In this case, $\exp(y - x) \gg 1$, and the term proportional to $\exp(y - x)$ in Eq. (A1) for A_{l0} in Appendix A is much larger than the other ones, which therefore can be neglected. To give an example, for $y = 10$ and $\gamma < 0.5$ where $y - x > 5$, the other terms in Eq. (A1) give relative contributions smaller than one percent. In Appendix A, it is shown that for $\exp(y - x) \gg 1$, the relative difference between the core-shell and the permeable particle scattering coefficient scales asymptotically as

$$\Delta A_{l0} \equiv \frac{A_{l0}(\gamma, y) - A_{l0}(0, y)}{A_{l0}(0, y)} \sim \frac{\gamma^{2l+1}}{y^2}, \qquad (18)$$

for a fixed value of $\gamma < 1$, and $y \to \infty$. Analogical estimations hold for the other scattering coefficients.

Summarizing, for $y - x > 5$, when $\exp(y - x) \gg 1$, our asymptotic analysis of the core-shell scattering coefficients performed in Appendix A results in the asymptotic scaling Eq. (18) for each scattering coefficient. This in turn, leads to the same scaling for all the hydrodynamic coefficients for core-shell suspensions at arbitrary concentration. Therefore, Eq. (18) justifies the conclusion that the core is practically insignificant for $y - x > 5$.

In earlier work, the hydrodynamic influence of the core was considered only for the intrinsic viscosity[21] and the translational diffusion coefficient[1] of a single core-shell particle, and for axisymmetric motion of core-shell particles along a common axis. They arrived at a conclusion similar to ours, namely, that the core is not sensed when the shell width sufficiently exceeds the penetration depth. We emphasize that we have given here the first systematic analysis of the core influence in concentrated systems.

V. CONCLUSIONS

A comprehensive theoretical analysis has been made of short-time dynamic properties in model suspensions of core-shell particles. Different from earlier theoretical work on core-shell systems where the influence of the core was analyzed mostly on the single-particle level, in this paper practically the full fluid-phase regime has been explored. We have achieved this using a versatile multipole simulation method of high accuracy. Our simulation results can be used, e.g., to test the accuracy of spherical cell model results for transport properties, frequently used in chemical engineering applications. In earlier work,[43] we showed that the cell model result[59] for the η_∞ of uniformly permeable spheres strongly overestimates its actual values at larger volume fractions. A similar overestimation can be expected for particles with a more complex structure.

The tabulated values listed in Appendix B are useful to colloid scientists working with core-shell-like systems, to estimate the influence of the shell permeability on short-time transport properties, and to construct approximate dynamic descriptions of permeable particles of different internal structures. The tables further allow for assessing the accuracy of generalized Stokes-Einstein relations, for core-shell particles where the core is hydrodynamically influential.

An essential result of our study is that for concentrated core-shell systems, the influence of the internal particle structure is significant. Even for hardly permeable shells, the core-shell systems are not accurately approximated by the impermeable hard-sphere model.

For concentrated systems of core-shell particles with a large shell permeability (small y), values of the transport coefficients depend significantly on the core size. However, we have found that for $\kappa(b - a) \gtrsim 5$, the core practically does not influence the considered transport properties, allowing for treating the particles as uniformly permeable spheres. The core criterion follows directly from our asymptotic analysis of all the scattering coefficients, which, in the employed accurate multipole method of calculating the multi-particle HIs in concentrated systems, are the only quantities which depend on the internal structure of the particles.

Our analysis of the core influence leads to the important conclusion that equilibrium diffusion measurements are, in a wide range of moderate and small shell permeabilities, not sensitive enough to resolve the internal hydrodynamic particle structure.

In this work, we have considered particles with excluded volume interactions only. Our general conclusions should remain valid when (core-shell) particles with additional pair interaction contributions, such as repulsive electrostatic and attractive van der Waals forces, are considered. There will be of course differences on a more quantitative level. For instance, our preliminary calculations for charge-stabilized particles indicate a fading influence of the permeability with increasing range of the electrostatic repulsion. Van der Waals attraction, on the other hand, increases the probability of near-contact configurations, thereby enhancing the importance of permeability effects.

While the precise form of the internal hydrodynamic structure is only weakly influential on equilibrium (short-time) dynamic suspension properties, this can be different in non-equilibrium situations. Two examples in case are the enhanced aggregation kinetics of attractive permeable particles in unstable colloidal suspensions,[60] and the permeability-induced suppression of lubrication-induced jamming hydro-clusters of particles in concentrated suspensions under strong shear flow. The hydrodynamic shear-thickening effect for hydro-clusters is taken advantage of in the design of soft-body armor composites.[14] The expressions for the core-shell scattering coefficients analyzed in this work can be usefully applied to study, e.g., the initial aggregate formation in unstable systems. This could be the topic of future work.

ACKNOWLEDGMENTS

The work of G.C.A. was supported by CAPES Foundation/Ministry of Education of Brazil. M.L.E.J. and E.W. were supported in part by the Polish Ministry of Science and Higher Education Grant No. N501 156538. G.N. thanks M. Heinen for helpful discussions and the Deutsche Forschungsgemeinschaft (SFB-TR6, project B2) for financial support.

Numerical simulations were done at NACAD-COPPE/UFRJ in Rio de Janeiro, Brazil, and at the Academic Computer Center in Gdansk, Poland.

APPENDIX A: SCATTERING COEFFICIENTS FOR CORE-SHELL PARTICLES

In Sec. II C, it has been explained that the self-diffusion, sedimentation and viscosity coefficients of concentrated suspensions depend on the particle model only through the single-particle friction operator $\mathbf{Z}_0$, which in turn is calculated with the use of the scattering coefficients $A_{l\sigma}$ and B_{l2}, with positive integer values of l and $\sigma = 0, 1, 2$.[34] Therefore, the dependence of the scattering coefficients on the particle model parameters (in our case, γ and y) is essential for the dynamics and rheology of concentrated suspensions.

The scattering coefficients for core-shell particles were evaluated by Cichocki and Felderhof in Ref. 23, and listed in their Eqs. (20)–(22). To facilitate taking the limit $\gamma \to 0$ of the core size going to zero, we rewrite these expressions, using a slightly different notation, as

$$A_{l0} = \frac{(2l+1)\,b^{2l-1}}{2\overline{D}_l}\left[(l+1)y^2\overline{P}_{l-1,l} + l\gamma^{2l-1}\overline{P}_{l+1,l}\right], \tag{A1}$$

$$A_{l1} = b^{2l+1}\left[1 + (2l+1)\frac{\overline{P}_{l,l}}{y^2\overline{P}_{l,l-1}}\right], \tag{A2}$$

$$A_{l2} = (2l+3)b^{2l+1}\left[\frac{1}{2l-1}\left(\frac{A_{l0}}{b^{2l-1}} - 1\right) + \frac{(2l+1)^2}{\overline{D}_l}\left(\overline{P}_{l-1,l} - 2x^{2l-1}\right)\right], \tag{A3}$$

$$B_{l2} = b^{2l+3}\left[\frac{2A_{l2}}{b^{2l+1}} - \frac{2l+3}{2l-1}\left(\frac{A_{l0}}{b^{2l-1}} - 1\right) - 1 + \frac{2(2l+1)(2l+3)}{ly^2}\left(1 - \frac{(2l+1)y^4\overline{P}_{l-1,l-2}}{\overline{D}_l}\right)\right], \tag{A4}$$

with

$$\overline{D}_l = (l+1)y^4\overline{P}_{l-1,l-2} + l(4l^2-1)\overline{P}_{l-1,l} + l\gamma^{2l-1}y^2\overline{P}_{l+1,l-2} - 4l(4l^2-1)x^{2l-1}, \tag{A5}$$

$$(-1)^{l+1}\overline{P}_{l,n} = R_l(x)R_n(-y)e^{y-x} - R_l(-x)R_n(y)e^{x-y}. \tag{A6}$$

For $m = 0, 1, 2, 3, \ldots$, the polynomials $R_m(z)$ are defined as

$$R_m(z) = z^m R\left(m + \frac{1}{2}, z\right) = \sum_{k=0}^{m}\frac{(m+k)!}{2^k k!(m-k)!}z^{m-k}, \tag{A7}$$

with the functions $R(m + 1/2, z)$ representing the modified spherical Bessel functions (see Sec. 10.2.11 in Abramowitz and Stegun[58]).

The polynomials $R_m(z)$ for lower values of $m \geq 0$ are explicitly

$$R_0(z) = 1, \tag{A8}$$

$$R_1(z) = z + 1, \tag{A9}$$

$$R_2(z) = z^2 + 3z + 3, \tag{A10}$$

$$R_3(z) = z^3 + 6z^2 + 15z + 15. \tag{A11}$$

For negative integer values of the index,

$$R_{-m}(z) = z^{-2m+1}R_{m-1}(z), \tag{A12}$$

where, in particular,

$$R_{-1}(z) = \frac{1}{z}. \tag{A13}$$

More specifically, the scattering coefficients determining the single-particle diffusion coefficients and the intrinsic viscosity in Eqs. (11)–(13) are of the form,[23]

$$A_{10} = \frac{3b}{2\overline{D}_1}\{(y-1)[2y^2 + \gamma(x^2+3x+3)]e^{y-x} + (y+1)[2y^2 + \gamma(x^2-3x+3)]e^{x-y}\}, \tag{A14}$$

$$A_{11} = \frac{b^3}{y^2}\frac{(x-1)(3+3y+y^2) + (1+x)(3-3y+y^2)e^{2(y-x)}}{(x-1) + (1+x)e^{2(y-x)}}, \tag{A15}$$

$$A_{20} = \frac{5b^3}{2\overline{D}_2}\{(y^2-3y+3)[3y^2(x+1) + 2\gamma^3(x^3+6x^2+15x+15)]e^{y-x} + (y^2+3y+3)[3y^2(x-1) + 2\gamma^3(x^3-6x^2+15x-15)]e^{x-y}\}, \tag{A16}$$

with

$$\overline{D}_1 = -12x + [2y^3+3y-3+x(x^2+3x+3)]e^{y-x} + [2y^3+3y+3+x(x^2-3x+3)]e^{x-y} \tag{A17}$$

$$\overline{D}_2 = -120x^3 + [3(x+1)(y^4+10y^2-30y+30) + 2\gamma x^2(x^3+6x^2+15x+15)]e^{y-x} + [3(x-1)(y^4+10y^2+30y+30) + 2\gamma x^2(x^3-6x^2+15x-15)]e^{x-y}. \tag{A18}$$

We recall that in Ref. 23, there are misprints in the expressions for A_{10} and A_{20}. We have given here the corrected expressions.

To estimate the hydrodynamic influence of the core for concentrated suspensions, we compare now the core-shell

scattering coefficients A_{l0} with arbitrary positive integer values of l, with their analogues for uniformly permeable spheres without a core but the same radius b and same permeability parameter $y = \kappa b$.

For typical experimental core-shell-like particle systems, the shell width is relatively large in comparison with the hydrodynamic penetration depth, i.e., $y - x = \kappa(b - a)$ is significantly larger than one. In this case, $e^{y-x} \gg 1$, and the terms proportional to e^{y-x} are much larger than the other ones, which therefore can be neglected. Under this condition, for arbitrary positive integer value of l we obtain

$$A_{l0}(\gamma, y) \approx \frac{(2l+1)b^{2l-1}}{2}\left[(l+1)+\frac{l\gamma^{2l-1}}{y^2}\frac{R_{l+1}(x)}{R_{l-1}(x)}\right] \cdot\left\{\frac{l(4l^2-1)}{y^2}+\frac{y^2R_{l-2}(-y)}{R_l(-y)}\left[(l+1)+\frac{l\gamma^{2l-1}}{y^2}\frac{R_{l+1}(x)}{R_{l-1}(x)}\right]\right\}^{-1}. \tag{A19}$$

TABLE I. Simulation results. Left: Translational self-diffusion coefficient $D_t(\gamma, y, \phi)/D_0^t(\gamma, y)$. Right: Rotational self-diffusion coefficient $D_r(\gamma, y, \phi)/D_0^r(\gamma, y)$.

	γ								γ						
ϕ	0.00	0.60	0.80	0.90	0.95	0.97	1.00	ϕ	0.00	0.60	0.80	0.90	0.95	0.97	1.00
	$y = 0$ (Annulus model)								$y = 0$ (Annulus model)						
0.05	1.000	0.988	0.963	0.941	0.926	0.920	0.908	0.05	1.000	0.999	0.994	0.986	0.979	0.975	0.966
0.15	1.000	0.963	0.887	0.822	0.779	0.759	0.724	0.15	1.000	0.997	0.980	0.954	0.930	0.917	0.888
0.25	1.000	0.936	0.811	0.705	0.636	0.604	0.546	0.25	1.000	0.994	0.963	0.916	0.874	0.850	0.796
0.35	1.000	0.908	0.734	0.592	0.501	0.459	0.383	0.35	1.000	0.991	0.944	0.873	0.809	0.773	0.690
0.45	1.000	0.878	0.658	0.486	0.380	0.331	0.243	0.45	1.000	0.987	0.921	0.825	0.738	0.689	0.576
	$y = 10$								$y = 10$						
0.05	0.947	0.946	0.943	0.935	0.925	0.919	0.908	0.05	0.987	0.987	0.986	0.983	0.978	0.975	0.966
0.15	0.842	0.839	0.829	0.805	0.776	0.758	0.724	0.15	0.958	0.958	0.955	0.945	0.928	0.916	0.888
0.25	0.739	0.734	0.717	0.679	0.631	0.602	0.546	0.25	0.925	0.924	0.919	0.900	0.870	0.849	0.796
0.35	0.641	0.634	0.610	0.558	0.495	0.458	0.383	0.35	0.886	0.885	0.877	0.849	0.804	0.772	0.690
0.45	0.551	0.541	0.510	0.446	0.372	0.329	0.243	0.45	0.842	0.841	0.830	0.792	0.731	0.687	0.576
	$y = 20$								$y = 20$						
0.05	0.929	0.929	0.929	0.927	0.923	0.919	0.908	0.05	0.980	0.980	0.980	0.979	0.977	0.974	0.966
0.15	0.789	0.788	0.786	0.781	0.768	0.756	0.724	0.15	0.934	0.934	0.933	0.931	0.923	0.915	0.888
0.25	0.654	0.653	0.649	0.640	0.619	0.599	0.546	0.25	0.881	0.881	0.879	0.875	0.861	0.846	0.796
0.35	0.529	0.527	0.521	0.509	0.480	0.453	0.383	0.35	0.820	0.820	0.818	0.811	0.790	0.767	0.690
0.45	0.417	0.414	0.407	0.390	0.355	0.324	0.243	0.45	0.753	0.753	0.750	0.741	0.712	0.681	0.576
	$y = 50$								$y = 50$						
0.05	0.917	0.917	0.917	0.917	0.916	0.916	0.908	0.05	0.973	0.973	0.973	0.973	0.973	0.972	0.966
0.15	0.751	0.751	0.751	0.750	0.749	0.746	0.724	0.15	0.911	0.911	0.911	0.911	0.910	0.908	0.888
0.25	0.593	0.593	0.592	0.590	0.588	0.584	0.546	0.25	0.839	0.839	0.839	0.838	0.837	0.833	0.796
0.35	0.447	0.447	0.445	0.443	0.440	0.433	0.383	0.35	0.757	0.757	0.757	0.756	0.753	0.748	0.690
0.45	0.320	0.320	0.318	0.315	0.310	0.302	0.243	0.45	0.669	0.668	0.667	0.666	0.662	0.655	0.576
	$y = 100$								$y = 100$						
0.05	0.913	0.913	0.913	0.913	0.913	0.912	0.908	0.05	0.970	0.970	0.970	0.970	0.970	0.970	0.966
0.15	0.738	0.738	0.737	0.737	0.737	0.737	0.724	0.15	0.901	0.901	0.901	0.901	0.901	0.900	0.888
0.25	0.570	0.570	0.570	0.569	0.569	0.568	0.546	0.25	0.821	0.821	0.820	0.820	0.820	0.819	0.796
0.35	0.416	0.416	0.416	0.415	0.414	0.413	0.383	0.35	0.729	0.729	0.729	0.728	0.727	0.727	0.690
0.45	0.284	0.283	0.283	0.281	0.280	0.278	0.243	0.45	0.629	0.629	0.629	0.628	0.627	0.626	0.576

For a uniformly permeable particle without a core, i.e., for $\gamma = 0$, we obtain

$$A_{l0}(0, y) \approx \frac{\frac{(2l+1)b^{2l-1}}{2}(l+1)}{\frac{l(4l^2-1)}{y^2} + \frac{y^2 R_{l-2}(-y)}{R_l(-y)}(l+1)}. \quad \text{(A20)}$$

The relative difference of the scattering coefficient with and without core is

$$\Delta A_{l0} \equiv \frac{A_{l0}(\gamma, y) - A_{l0}(0, y)}{A_{l0}(0, y)} = \frac{\frac{l^2(4l^2-1)\gamma^{2l-1}}{(l+1)y^4}\frac{R_{l+1}(x)}{R_{l-1}(x)}}{\frac{l(4l^2-1)}{y^2} + \left[l+1+\frac{l\gamma^{2l-1}}{y^2}\frac{R_{l+1}(x)}{R_{l-1}(x)}\right]\frac{y^2 R_{l-2}(-y)}{R_l(-y)}}, \quad \text{(A21)}$$

and scales thus asymptotically as

$$\Delta A_{l0} \sim \frac{\gamma^{2l+1}}{y^2}, \quad \text{(A22)}$$

for a fixed value of γ and $y \to \infty$.

We have derived similar expressions for the other scattering coefficients, $A_{l,\sigma}$ and B_{l2}, with $\sigma = 1, 2$ and arbitrary positive integer values of l. An analogous asymptotic analysis applies to all the other scattering coefficients, and therefore, also to the single-particle friction operator $\mathbf{Z}_0$ and, as it follows from the method described in Sec. II C, to all the transport coefficients of concentrated suspensions.

APPENDIX B: TABLES

Tables I and II list our high-precision simulation results for the short-time transport coefficients normalized by their limiting values at $\phi = 0$, i.e., for D_t/D_0^t, D_r/D_0^r, K, and η_∞/η_0, as functions of $\{\gamma, y, \phi\}$, for volume fractions up to $\phi = 0.45$, and core-to-particle radius ratio $\gamma = a/b$ from zero (uniformly permeable spheres of radius b)

TABLE II. Simulation results. Left: Sedimentation coefficient $K(\gamma, y, \phi)$. Right: Effective viscosity $\eta_\infty(\gamma, y, \phi)/\eta_0$.

	γ								γ						
ϕ	0.00	0.60	0.80	0.90	0.95	0.97	1.00	ϕ	0.00	0.60	0.80	0.90	0.95	0.97	1.00
	$y = 0$ (Annulus model)								$y = 0$ (Annulus model)						
0.05	1.000	0.841	0.785	0.755	0.740	0.733	0.724	0.05	1.00	1.03	1.07	1.10	1.12	1.13	1.14
0.15	1.000	0.613	0.492	0.435	0.405	0.393	0.376	0.15	1.00	1.08	1.22	1.33	1.42	1.46	1.53
0.25	1.000	0.466	0.319	0.254	0.223	0.211	0.192	0.25	1.00	1.14	1.39	1.64	1.84	1.95	2.17
0.35	1.000	0.366	0.211	0.148	0.121	0.110	0.0949	0.35	1.00	1.21	1.60	2.06	2.48	2.73	3.33
0.45	1.000	0.296	0.142	0.0864	0.0642	0.0562	0.0448	0.45	1.00	1.27	1.84	2.61	3.45	4.01	5.65
	$y = 10$								$y = 10$						
0.05	0.763	0.761	0.757	0.749	0.738	0.733	0.724	0.05	1.09	1.09	1.10	1.11	1.12	1.13	1.14
0.15	0.451	0.448	0.439	0.422	0.403	0.393	0.376	0.15	1.30	1.31	1.32	1.37	1.42	1.46	1.53
0.25	0.276	0.270	0.260	0.241	0.221	0.210	0.192	0.25	1.57	1.57	1.62	1.72	1.86	1.96	2.17
0.35	0.174	0.167	0.155	0.137	0.119	0.110	0.0949	0.35	1.89	1.91	1.99	2.20	2.52	2.74	3.33
0.45	0.114	0.106	0.0937	0.0774	0.0630	0.0560	0.0448	0.45	2.30	2.33	2.48	2.88	3.53	4.04	5.65
	$y = 20$								$y = 20$						
0.05	0.742	0.742	0.741	0.740	0.736	0.732	0.724	0.05	1.11	1.11	1.11	1.12	1.12	1.13	1.14
0.15	0.411	0.410	0.409	0.406	0.399	0.391	0.376	0.15	1.40	1.40	1.40	1.41	1.44	1.46	1.53
0.25	0.230	0.229	0.227	0.224	0.216	0.209	0.192	0.25	1.79	1.80	1.81	1.83	1.90	1.97	2.17
0.35	0.129	0.128	0.126	0.122	0.115	0.109	0.0949	0.35	2.35	2.35	2.38	2.45	2.61	2.78	3.33
0.45	0.0730	0.0712	0.0690	0.0658	0.0600	0.0552	0.0448	0.45	3.13	3.14	3.20	3.35	3.71	4.11	5.65
	$y = 50$								$y = 50$						
0.05	0.730	0.730	0.730	0.729	0.729	0.729	0.724	0.05	1.13	1.13	1.13	1.13	1.13	1.13	1.14
0.15	0.388	0.388	0.387	0.387	0.387	0.386	0.376	0.15	1.47	1.47	1.47	1.48	1.48	1.48	1.53
0.25	0.206	0.206	0.206	0.206	0.205	0.204	0.192	0.25	2.00	2.00	2.00	2.00	2.01	2.02	2.17
0.35	0.107	0.107	0.107	0.106	0.106	0.105	0.0949	0.35	2.82	2.82	2.83	2.85	2.87	2.91	3.33
0.45	0.0542	0.0539	0.0535	0.0532	0.0528	0.0519	0.0448	0.45	4.17	4.18	4.21	4.26	4.33	4.45	5.65
	$y = 100$								$y = 100$						
0.05	0.727	0.727	0.727	0.727	0.727	0.726	0.724	0.05	1.13	1.13	1.13	1.13	1.13	1.13	1.14
0.15	0.382	0.382	0.381	0.381	0.381	0.381	0.376	0.15	1.50	1.50	1.50	1.50	1.50	1.50	1.53
0.25	0.199	0.199	0.199	0.199	0.199	0.199	0.192	0.25	2.08	2.08	2.08	2.08	2.08	2.08	2.17
0.35	0.101	0.101	0.101	0.101	0.101	0.101	0.0949	0.35	3.05	3.05	3.05	3.06	3.06	3.07	3.33
0.45	0.0492	0.0491	0.0490	0.0490	0.0489	0.0488	0.0448	0.45	4.76	4.77	4.79	4.81	4.84	4.87	5.65

to one (non-permeable spheres of radius b). Values of the outer radius to penetration depth ratio, $y = \kappa b$, are considered from very small values characteristic of a highly permeable shell, including the spherical annulus model limit $y = 0$, up to $y = 100$, where the shell is only very weakly permeable. In the zero-penetration limit $y \to \infty$, we recover non-permeable hard spheres of radius b, which are also (equivalently) described by taking $\gamma = 1$ (see the last column in the tables below). For $\gamma = 0$ (the first column), uniformly permeable spheres of radius b are recovered. These limiting cases have been thoroughly analyzed over an extended concentration range in our previous publications.[40–45] The special case $\gamma = 0$ and $y = 0$ should be understood as the single-particle limit. All the listed values will be quite useful both to experimentalists and theoreticians dealing with the (hydro)dynamics of core-shell particles systems.

The numerical procedure, described in details in Sec. II D, has been adjusted in such a way that the relative accuracy of all the transport coefficients listed in the tables is of the order of 1% or better (for sedimentation), or of the order of 0.5% or better (for the translational and rotational self-diffusion and effective viscosity).

[1] J. Masliyah, G. Neale, K. Malysa, and T. G. M. van de Ven, Chem. Eng. Sci. **42**, 245 (1987).
[2] M. H. G. Duits, P. A. Nommensen, D. van den Ende, and J. Mellema, Colloids Surf., A **183–185**, 335 (2001).
[3] A. Kasper, E. Bartsch, and H. Sillescu, Langmuir **14**, 5004 (1998).
[4] G. Petekidis, J. Gapiński, P. Seymour, J. S. van Duijneveldt, D. Vlassopoulos, and G. Fytas, Phys. Rev. E **69**, 042401 (2004).
[5] M. Zackrisson, A. Stradner, P. Schurtenberger, and J. Bergenholtz, Langmuir **21**, 10835 (2005).
[6] M. Zackrisson, A. Stradner, P. Schurtenberger, and J. Bergenholtz, Phys. Rev. E **73**, 011408 (2006).
[7] B. Loppinet, G. Fytas, D. Vlasssopoulos, C. N. Likos, G. Meier, and G. J. Liu, Macromol. Chem. Phys. **206**, 163 (2005).
[8] H. Nakamura and K. Tachi, J. Appl. Polym. Sci. **102**, 2212 (2006).
[9] G. A. Buxton and N. Clarke, Soft Matter **3**, 1513 (2007).
[10] P. Voudouris, J. Choi, H. Dong, M. R. Bockstaller, K. Matyjaszewski, and G. Fytas, Macromolecules **42**, 2721 (2009).
[11] M. Sedlacik, V. Pvalinek, P. Saha, P. Svrcinova, F. Filip, and J. Stejskal, Smart Mater. Struct. **19**, 115008 (2010).
[12] P. N. Segrè, O. P. Behrend, and P. N. Pusey, Phys. Rev. E **52**, 5070 (1995).
[13] C. N. Likos, H. Löwen, M. Watzlawek, B. Abbas, O. Jucknischke, J. Allgaier, and D. Richter, Phys. Rev. Lett. **80**, 4450 (1998).
[14] N. J. Wagner and J. F. Brady, Phys. Today **62**(10), 27 (2009).
[15] H. C. Brinkman, Appl. Sci. Res., Sec. A **1**, 27 (1947).
[16] P. Debye and A. M. Bueche, J. Chem. Phys. **16**, 573 (1948).
[17] B. U. Felderhof and R. B. Jones, Physica A **93**, 457 (1978).
[18] R. Reuland, B. U. Felderhof, and R. B. Jones, Physica A **93**, 465 (1978).
[19] A. A. Potanin and W. B. Russel, Phys. Rev. E **52**, 730 (1995).
[20] S. L. Elliot and W. B. Russel, J. Rheol. **42**, 361 (1998).
[21] M. Zackrisson and J. Bergenholtz, Colloids Surf., A **225**, 119 (2003).
[22] S. B. Chen and X. Ye, J. Colloid Interface Sci. **221**, 50 (2000).
[23] B. Cichocki and B. U. Felderhof, J. Chem. Phys. **130**, 164712 (2009).
[24] W. van Saarloos, Physica A **147**, 280 (1987).
[25] S. Veerapaneni and M. R. Wiesner, J. Colloid Interface Sci. **177**, 45 (1996).
[26] B. U. Felderhof, Physica A **80**, 63 (1975).
[27] J. M. Deutch and B. U. Felderhof, J. Chem. Phys. **62**, 2398 (1975).
[28] R. B. Jones and R. Schmitz, Physica A **149**, 373 (1988).
[29] J. L. Anderson, P. F. McKenzie, and R. M. Webber, Langmuir **7**, 162 (1991).
[30] J. L. Anderson and Y. Solomomentsev, Chem. Eng. Commun. **148-150**, 291 (1996).
[31] Y. Solomomentsev, A. Kotov, and V. Starov, Int. J. Multiphase Flow **18**, 739 (1992).
[32] J. Kuo and H. J. Keh, J. Colloid Interface Sci. **195**, 353 (1997).
[33] S. B. Chen, Phys. Fluids **10**, 1550 (1998).
[34] B. Cichocki, B. U. Felderhof, and R. Schmitz, PhysicoChem. Hydrodyn. **10**, 383 (1988).
[35] P. A. Nommensen, M. H. G. Duits, D. van den Ende, and J. Mellema, Phys. Rev. E **59**, 3147 (1999).
[36] J. Happel and H. Brenner, *Low Reynolds Number Hydrodynamics* (Martinus Nijhoff, Dordrecht, 1986).
[37] S. Kim and S. J. Karrila, *Microhydrodynamics: Principles and Selected Applications* (Butterworth-Heinemann, London, 1991).
[38] B. Cichocki, B. U. Felderhof, K. Hinsen, E. Wajnryb, and J. Bławzdziewicz, J. Chem. Phys. **100**, 3780 (1994).
[39] B. Cichocki, M. L. Ekiel-Jeżewska, and E. Wajnryb, J. Chem. Phys. **111**, 3265 (1999).
[40] G. C. Abade, B. Cichocki, M. L. Ekiel-Jeżewska, G. Nägele, and E. Wajnryb, J. Chem. Phys. **132**, 014503 (2010).
[41] G. C. Abade, B. Cichocki, M. L. Ekiel-Jeżewska, G. Nägele, and E. Wajnryb, Phys. Rev. E **81**, 020404(R) (2010).
[42] G. C. Abade, B. Cichocki, M. L. Ekiel-Jeżewska, G. Nägele, and E. Wajnryb, J. Phys.: Condens. Matter **22**, 322101 (2010).
[43] G. C. Abade, B. Cichocki, M. L. Ekiel-Jeżewska, G. Nägele, and E. Wajnryb, J. Chem. Phys. **133**, 084906 (2010).
[44] B. Cichocki, M. L. Ekiel-Jeżewska, G. Nägele, and E. Wajnryb, Phys. Fluids **23**, 083303 (2011).
[45] G. C. Abade, B. Cichocki, M. L. Ekiel-Jeżewska, G. Nägele, and E. Wajnryb, J. Chem. Phys. **134**, 244903 (2011).
[46] R. G. Cox and H. Brenner, J. Fluid Mech. **28**, 391 (1967).
[47] P. Mazur and D. Bedeaux, Physica **76**, 235 (1974).
[48] B. U. Felderhof, Physica A **84**, 569 (1976).
[49] H. Hasimoto, J. Fluid Mech. **5**, 317 (1959).
[50] B. Cichocki and B. U. Felderhof, J. Chem. Phys. **94**, 556 (1991).
[51] A. S. Khair and J. S. Brady, J. Rheol. **49**, 1449 (2005).
[52] H. Zhang and G. Nägele, J. Chem. Phys. **117**, 5908 (2002).
[53] B. Cichocki, M. L. Ekiel-Jeżewska, P. Szymczak, and E. Wajnryb, J. Chem. Phys. **117**, 1231 (2002).
[54] P. Szymczak and B. Cichocki, J. Stat. Mech.: Theory Exp. **2008**, P0125.
[55] B. Cichocki, M. L. Ekiel-Jeżewska, and E. Wajnryb, J. Chem. Phys. **119**, 606 (2003).
[56] B. Cichocki, B. U. Felderhof, and R. Schmitz, Physica A **154**, 233 (1989).
[57] M. L. Ekiel-Jeżewska and E. Wajnryb, "Precise multipole method for calculating hydrodynamic interactions between spherical particles in the Stokes flow," in *Theoretical Methods for Micro Scale Viscous Flows*, edited by F. Feuillebois and A. Sellier (Transworld Research Network, Kerala, 2009).
[58] M. Abramowitz and I. A. Stegun, *Handbook of Mathematical Functions* (Dover, New York, 1965).
[59] H. Ohshima, Colloids Surf., A **347**, 33 (2009).
[60] P. G. Wolynes and J. A. McCammon, Macromolecules **10**, 86 (1977).
[61] R. J. Phillips, J. F. Brady, and G. Bossis, Phys. Fluids **31**, 3462 (1988).
[62] A. J. C. Ladd, J. Chem. Phys. **93**, 3484 (1990).
[63] G. Mo and A. S. Sangani, Phys. Fluids **6**, 1637 (1994).
[64] M. H. J. Hagen, D. Frenkel, and C. P. Lowe, Physica A **272**, 376 (1999).
[65] A. Sierou and J. F. Brady, J. Fluid Mech. **448**, 115 (2001).
[66] A. J. Banchio and J. F. Brady, J. Chem. Phys. **118**, 10323 (2003).
[67] A. J. Banchio and G. Nägele, J. Chem. Phys. **128**, 104903 (2008).
[68] Note that in Ref. 23, there are misprints in Eqs. (28) and (32); however, the full expressions in Eq. (20) of this reference are correct.